PHOTONICS Research

Manipulating light radiation from a topological perspective

Xuefan Yin and Chao Peng*

State Key Laboratory of Advanced Optical Communication Systems and Networks, Department of Electronics, Peking University, Beijing 100871, China
*Corresponding author: pengchao@pku.edu.cn

Received 22 July 2020; revised 31 August 2020; accepted 2 September 2020; posted 2 September 2020 (Doc. ID 403444); published 21 October 2020

Manipulating radiation is important for a variety of optoelectronic applications, such as on-chip lasers, energy-efficient grating couplers, and antennas for light detection and ranging. Although designing and optimizing those optoelectronic devices are usually believed to be an engineering-oriented task, recent research reveals that the principles underlying radiation manipulation are closely connected to the concept of topology—the study of properties that are invariant under continuous deformations. In this review, we summarize a series of advances of the physics, phenomena, and applications related to radiation manipulation, in which topological concepts were adopted. Radiation could carry energy escaping from the system, breaking the energy conservation. The non-Hermiticity of such systems brings quite different physical consequences when comparing with the Hermitian counterparts and, hence, also results in the emergence of many interesting and extraordinary phenomena. In particular, it is found that the perfect trapping of light can still be realized in such non-Hermitian systems because of the photonic realization of bound states in the continuum. The fundamental nature of bound states in the continuum has been identified to be topological: they are essentially topological defects of the polarization vector field in momentum space, depicted by a kind of topological invariant named topological charges. Therefore, manipulation of radiation channels can be realized by controlling the topological charge evolution in momentum space. It is also demonstrated that the photonic states accompanied with different topological charges generate vortex beams with unique far-field radiation patterns, and ultra-fast switching of such vortex beams is demonstrated according to this principle. The progresses of topological photonics upon light radiation show that the topology is not just mathematical convenience for depicting photonic systems, but has brought realistic consequences in manipulating light and will boost the applications of photonics and optoelectronics in many aspects.

https://doi.org/10.1364/PRJ.403444

1. INTRODUCTION

Over the last decade, topological photonics [1–4] appeared as a rapidly emerging field of research, in which topological ideas are exploited to design and control the behavior of light, thus boosting the discovery of fundamentally novel phenomena and potentially revolutionary applications such as back-scattering-immune waveguides [5,6], disorder-insensitive delay lines [7,8], and topological lasers [9–11] with enhanced single-mode stability.

As a branch of mathematics, topology deals with robust conserved quantities that do not change when objects are continuously deformed. The ideas of using topological concepts to depict the geometric properties of physical systems originate from the discovery of the integer quantum Hall effect (IQHE) [12]. In this case, when two-dimensional (2D) electrons whose energy sits within the energy gap between landau levels interact with an external magnetic field, it gives rise to quantized Hall conductance. Such quantization is related to a topological invariant known as the Chern invariant (TKNN invariant, after Thouless, Kohomoto, Nightingale, and den Nijs [13]) that can be understood in terms of Bloch wave functions as a surface integral of the Berry curvature in momentum space over the Brillouin zone (BZ). Therefore, the Chern invariant characterizes the quantized geometric properties and the global behavior of wave functions on the entire bulk energy band.

IQHE as well as the Chern invariant boosts the emergence of topological insulators [14,15]: gapless conducting states exist at the interfaces (edges or surfaces) when the Chern invariant changes. Importantly, since the time-reversal (TR) symmetry has been broken by the external magnetic field, these electronic states are chiral, propagating in one direction along the

interface with the TR counterpart disallowed. The existence of such unidirectional interface states is deeply related to the topology of bulk bands, ruled by the bulk-boundary correspondence [16–18], which can be understood in a brief picture: since the integer topological invariant of individual bands persists under perturbations or deformations unless the energy gap is closed, the energy gap has to be vanished at the interface between two domains whose topological invariants are different, leading to the appearance of localized states stuck in the interface. In this way, bulk-boundary correspondence is established that describes how bulk topology affects the characteristics of states at the boundaries.

In addition to the IQHE, another class of topological phases was discovered in 2005 [19,20], which is the quantum spin Hall effect (QSHE) [21]. When TR symmetry is preserved, the total Chern invariants are trivial. However, once the spin-orbit coupling is present, the wave functions and bulk energy band can be characterized by another nontrivial binary (Z2) topological invariant [20,22]: spin-Chern numbers. Since the two spin components of electrons are TR pairs, as long as there are no spin-slip perturbations, the two spin components are decoupled from each other, protected by the TR symmetry, and independently behave as a Chern insulator with paired and opposite Chern invariants, each encoded by the spin-Chern number. As a result, at the interface between two topologically inequivalent domains, the edge states in two spin states are always paired as TR counterparts of each other, propagating in opposite directions with spin-momentum locking. This kind of systems is named quantum spin Hall systems or Z2 topological insulators [23–29].

Inspired by the QSHE insulators protected by TR symmetry, other topological phases under various symmetries are investigated in condensed-matter physics, giving rise to different symmetry-protected topological (SPT) invariants [30]. Examples include the valley Chern number in valleytronics [31–36], spin-valley Chern number under spin-valley locking [37,38], winding number [39,40] in the one-dimensional (1D) Su–Schrieffer–Heeger (SSH) model [41] with chiral symmetry, and mirror Chern number [42–44] resulting from crystalline symmetry [45]. Although the definitions of these topological invariants are different, they all encode the topological phases of the bulk energy band and result in gapless edge states that are ruled by bulk-boundary correspondence under some relevant symmetries. Note that SPT orders are conserved quantities only when deformations do not break the relevant symmetry. Once the symmetry is broken, SPT orders would fail to guarantee the topological protection of the boundaries, and thus the gapless edge states would disappear even if the gap is still open.

Topological phases of matter, although rooted in condensed-matter systems, were proved to be a ubiquitous property in a wide range of wave systems in 2008 [46]. After that, topological ideas were expanded to other wave systems, for example, photonic systems. As a classic optical analog of electrons in quantum systems, the photonic system obtains the benefits of flexibility and diversity, thus becoming a good candidate to realize exotic topological models and investigate the fundamental mechanisms behind them. Following a realistic demonstration of the quantum Hall effect in photonics [5], further progresses towards the implementation of topological models have been achieved in the optical domain, giving rise to the emergence of a new branch of physics as topological photonics.

However, compared to the physics of electrons in solids, there are some unique features of photonic systems. Different from the electrons that obey Fermi statistics, the photons are bosonic. This fundamental distinction leads to impacts on many aspects. First, photons are neutral boson with integer spin, which do not experience the magnetic field directly. Second, photons acts differently under TR operator $\mathcal{T}$, satisfying $\mathcal{T}^2 = 1$ rather than $\mathcal{T}^2 = -1$ [47,48]; the latter one ensuring Kramer's degeneracy for electrons. Therefore, photons have different topological classifications from electrons with respect to $\mathcal{T}$. Most importantly, photons are non-conserved particles with finite lifetimes in most realistic optical devices, subjected to a variety of non-equilibrium processes ranging from the gains and absorptions of medium material to the radiation losses caused by open photonic boundaries or defects that break the topological protection [49]. Namely, the realistic photonic systems are non-Hermitian in general.

Obviously, the non-Hermiticity brought by these non-equilibrium processes provides extra degrees of freedom (DOFs) and gives rise to intrinsically different physics compared to their Hermitian counterparts [50]. First of all, the non-Hermitian system leads to complex energy bands in general, then how to extend the concept of "band gap" from Hermitian system becomes the first obstacle. In this case, real and imaginary parts of eigenvalues co-exist but are not "gapped" at the same time. To address this problem, several proposals have been made. For example, "separable," "isolated," and "inseparable" bands are defined based on their complex eigenvalues [51].

Second, the complex energy bands give rise to a particular class of singularities: the exceptional points (EPs) [52,53]. At the EPs, not only the eigenvalues but also eigenstates coalesce and the system Hamiltonian becomes non-diagonalizable, leading to a variety of fancy phenomena. For example, in a whispering-gallery-mode (WGM) resonator, modes in the vicinity of EPs are found to become chiral, which can be employed to realize the unidirectional lasing [54]. Like its Hermitian counterparts, Dirac points [19,55,56] and Weyl points [57–59], along a closed loop encircling the EP, nontrivial geometric phase is gained, known as global Berry phase [60–62]. In parity ($\mathcal{P}$)-time ($\mathcal{T}$) symmetric systems [63,64], EPs are known as the spontaneously $\mathcal{PT}$ symmetry-broken points [65], resulting in sophisticated geometry of energy bands. On the other hand, the existence of EPs also results in anomalous behavior of edge states [66]. Different from conventional Chern numbers in the Hermitian system, several new kinds of winding numbers with different physical implications are employed to characterize the topology of EPs [51,66,67]. As the diagonalizability-broken points of the system, EPs are generally considered to be sensitive to parameters. Nevertheless, a kind of symmetry-protected EPs are reported, characterized by topological defects of a vector field defined by average values of Pauli matrices [68].

In addition to the EPs, another unique concept in non-Hermitian physics is the spectral singularity [69,70], at which the diagonalizability of the system Hamiltonian with a continuous spectrum has been broken. In a scattering system, the

transmission or reflection coefficients at spectral singularities tend to infinity, and the persistent wave emission scattering dynamics are observed [71]. The input-direction-independent unidirectional light wave propagation and single-direction lasing have also been demonstrated at spectral singularities [72].

Thirdly, a finite but arbitrarily large amount of eigenstates in the non-Hermitian system are found to be localized at the boundary even when the system has no disorders. This anomalous localization, named the non-Hermitian skin effect [73–77], has been discussed in the system with high-order EPs [78] or open boundaries [74]. Moreover, bulk bands in the non-Hermitian system are more sensitive to boundaries due to the presence of the imaginary magnetic flux under the periodical boundary condition [67,76]. These exotic phenomena lead to the breakdown of conventional bulk-boundary correspondence [74,79–81], which necessitates the redefinition of related topological invariants as well as new classifications of non-Hermitian topological phases [82–84]. For example, new topological invariants like half-integer charges associated with EPs [66,85], non-Bloch winding numbers [73], and non-Bloch Chern invariants [74] were introduced to interpret the geometries of non-Hermitian energy bands, and the achievements on the classification of non-Hermitian topological phases also have been made [86]. Recently, this novel non-Hermitian skin effect and anomalous bulk-boundary correspondence have been demonstrated in the non-Hermitian quantum walk system experimentally [87,88].

In spite of many breakthroughs on the interplay between band topology and non-Hermiticity, there is another regime of topological photonics that studies the topology of radiation. Optical radiations create leaky and open channels and thus bring non-Hermiticity to photonic systems. It is found that the bound states in continuum (BICs) [89–91], a ubiquitous phenomenon in non-Hermitian wave systems, can be reinterpreted as topological defects [92] of the polarization vector field in momentum space, featuring a new kind of topological invariant defined in the radiation field named topological charge. Afterward, half-integer topological charges were observed, arising from the bulk Fermi arcs around paired EPs [93]. This crucial observation shows that the features of bands and wave functions (i.e., BICs and EPs) are connected to the topology of the radiation field and then reveals a new perspective to investigate the non-Hermitian photonic system: we can observe the far-field radiation to probe and exploit the topological phases underlying the energy bands.

On the other hand, topological perspective also affords new possibilities in manipulating radiation—the main topic of this review. The characteristics of radiation in photonic systems can be interpreted by topological concepts as well as controlled by topological invariants, and thus they offer new perspectives and mythologies in manipulating light. Considering that optical radiation plays such a crucial role in varieties of photonic devices ranging from lasers, sensors, to optical inputs/outputs (IOs), we believe that these progresses would pave the way to radiation manipulation and boost the emergence and development of novel optoelectronic applications.

The rest of this review is organized as follows. In Section 2, we provide an overview of the topological concepts in the non-Hermitian system, with a brief review of topological invariants in both Hermitian and non-Hermitian systems first and the key fingerprints of non-Hermitian photonics, including BICs and EPs. In Section 3, we summarize a series of recent works on manipulating radiation from topological charge evolution. In Section 4, the latest progresses on manipulating radiation wave-fronts from topological concepts are discussed, and we focus on the vortex/vector beam generation and manipulation. In Section 5, we conclude our remarks.

2. TOPOLOGICAL CONCEPTS IN NON-HERMITIAN PHOTONICS

A. Topological Invariants for Bulk Bands

Before starting the discussion upon the topology of radiation, we first present a brief review of conventional topological invariants in band topology. The first topological invariants employed in condensed-matter physics, as the TKNN invariants [13], are Chern numbers. In 2D systems, if the Hamiltonian has the spatial periodicity, the geometry of the eigenstates in momentum space can be described by the local Berry connection $A_n(k) = i\langle u_n(k)|\nabla_k|u_n(k)\rangle$ and Berry curvature defined in the Bloch states as $\mathbf{\Omega}_n(k) = \nabla_k \times A_n(k)$, in which $u_n(k)$ is the Bloch states at band n with crystal momentum k. Note that Berry curvature can be also defined in other parameter space. Further, the Chern number can be defined as the integral of Berry curvature over the whole first BZ:

$$C_n = \frac{1}{2}\int_{\mathrm{BZ}} \mathrm{d}^2 k \mathbf{\Omega}_n(k). \tag{1}$$

Once the phase of the Bloch states cannot be continuously defined, nonzero Berry curvature occurs, and Chern numbers must necessarily be nonzero, too, according to Stokes' theorem. In this way, the Chern number encodes the geometric properties of the bands in the whole momentum space. As for the conventional quantum Hall effect, the Chern numbers are always integers, while for systems with strong interaction and disorders, fractional Chern numbers can be found to manifest the fractional quantum Hall effect [94]. In three-dimensional (3D) topological systems, the point degeneracy of energy bands, Weyl points [57–59,95,96], also exhibit nonzero Chern numbers. In higher-dimensional quantum Hall systems with even numbers of spatial dimensions, for example, the four-dimensional (4D) systems [97,98], new types of quantum Hall effects emerge, characterized by second Chern numbers, in contrast to first Chern numbers stated above in systems with lower dimension.

Besides the Chern numbers, other topological invariants were derived to depict the topological phases under certain symmetries as SPT orders. For example, spin-Chern numbers [19,20] are defined to describe the geometry of spin states, which can be considered as Chern numbers accounting only for one spin component. The whole spin-Chern numbers of the entire band can be written as

$$C_s = \frac{1}{2}(C_n^{\uparrow} - C_n^{\downarrow}), \tag{2}$$

in which the superscript denotes the spin component. The coefficient 1/2 comes from the binary symmetry of the QSHE. Similarly, valley-Chern numbers [31,32] can be considered as

Chern numbers, accounting only for a single valley. In the honeycomb lattice, which is the optical analog of graphene, there are two different valleys at K and K' points in momentum space; therefore, the valley-Chern numbers for a single valley are defined as

$$C_n^{K,K'} = \frac{1}{2}\int_{\mathrm{HBZ}} \mathrm{d}^2 k \Omega_n(k). \tag{3}$$

Here, HBZ denotes half-BZ, including the single valley at the K or K' point. Then, the whole valley-Chern number can be written as $C_V = C_n^K - C_n^{K'}$. Note that multi SPT orders can be simultaneously applied to bulk bands to describe the topological phase. For example, in the valley photonic crystal (VPC) [37,38], incorporating the valley DOF and spin DOF results in spin-valley Chern numbers [30], accounting for the geometries of bulk bands of certain spin states in the single valley.

Obviously, all of these topological invariants are defined upon wave functions, depicting the geometry of eigenstates of bulk bands under certain symmetries. According to bulk-boundary correspondence, these topological invariants also govern the behavior of gapless eigenstates confined in the interface between two topologically inequivalent domains. Similar definitions of topological invariants can also be found in the 1D SSH model with chiral symmetry [39,40] and 3D lattice with mirror symmetry [44,45].

When topological concepts are expanded from condensed-matter systems to photonics, one major problem is the non-Hermiticity, since gain and loss are more common in photons than in electrons. For general non-Hermitian systems, conventional bulk-boundary correspondence is disabled by non-equilibrium processes [74,79–81], making edge modes no longer strictly tied to bulk Chern numbers and giving rise to some exotic phenomena such as anomalous localization of eigenstates at boundaries due to the non-Hermitian skin effect [73,75–77]. To address these problems, some researchers revealed that the breakdown of conventional bulk-boundary correspondence stems from the non-Bloch-wave nature [74,81] of eigenstates in the open-boundary system. They introduced non-Bloch Chern numbers defined in the 2D generalized BZ with complex-value wave vectors [74]:

$$C_n = \frac{1}{2\pi i}\int_{\tilde{T}^2} \mathrm{d}^2 \tilde{k} \epsilon^{i,j} \langle \partial_i u_{Ln}(\tilde{k}) | \partial_j u_{Rn}(\tilde{k}) \rangle, \quad i,j \in (x,y). \tag{4}$$

Here, $\tilde{k}$ denotes the complex-valued momentum, parametrizing a generalized BZ $\tilde{T}$, deformation from the standard BZ T into complex spaces. Coefficient $\epsilon^{i,j} = \delta_{i,j}$. $u_{Rn}(\tilde{k})$ and $u_{Ln}(\tilde{k})$ are right and left eigenvectors of the non-Bloch Hamiltonian, obeying the bi-orthogonal normalization condition $\langle u_{Lm} | u_{Rn} \rangle = \delta_{mn}$. In this proposal, the revised Chern number can be considered as the conventional Chern number of the non-Bloch Hamiltonian $\tilde{H}(\tilde{k})$ rather than conventional $H(k)$. The same non-Bloch Chern numbers can also be applied to the 1D non-Hermitian SSH model. On the other hand, some other researchers revealed that EPs can give rise to similar anomalous localization effects [78], and revised Chern numbers associated with EPs are employed to give a geometrical interpretation to the localized states.

B. Features of Optical Radiation and Topological Charges

In all of the non-equilibrium processes affecting the behavior of photons in non-Hermitian systems, optical radiation attracts much attention since it governs the energy exchange in most of the realistic optoelectronic devices. One typical case of such open photonic systems is the photonic crystal (PhC) slabs [99,100] shown in Fig. 1(a). As a general and versatile platform, PhC slabs afford varieties of photonic applications, such as filters, lasers, waveguides, and cavities, in which optical radiation plays a crucial role as channels for energy in and out.

Beyond the Hermitian framework, there are several unique features of non-Hermitian systems due to optical radiation, which do not have the Hermitian counterparts. The first one is the BICs [89–91]—the modes whose lifetimes remain infinite with open radiation channels and allowable couplings to the continuum. In literature, photonic BICs were thought to be grouped into two types: BICs with symmetry protection and tunable BICs robust in momentum space. At first, the lack of a comprehensive picture in understanding the radiation had resulted in a challenge for unifying two types of BICs. Some semi-analytical methods for non-Hermitian photonics were proposed to make clear the fundamental mechanisms of BICs [101–105], and the nature of BICs in PhC slabs has been identified to be topological; they are essentially topological defects [92] of the polarization vector field in momentum space [106,107] [Figs. 1(b) and 1(c)]. Topological defects are indeed ubiquitous phenomena: examples range from quantum vortices in superfluids to singular optical beams [108], which are characterized by the nontrivial winding patterns of system parameters (velocity, phase, or polarization) in real space. For the BICs in open photonics specifically, the topological charge (q) carried by topological defects in momentum space is defined as the winding of polarization directions around a specific state as [106]

$$q = \frac{1}{2}\oint_C \mathrm{d}k \cdot \nabla_k \theta(k). \tag{5}$$

Here, $\theta(k)$ is the angle of major axes of the polarization vector that depicts the radiation field $\psi(k) = \arg[e_x\hat{x} + ie_y\hat{y}]$, and C is a closed simple path in momentum space that goes around the state in the counterclockwise (CCW) direction. Topological charges defined in radiation have a similar form to the Chern numbers defined in bulk bands, and they depict the geometry of far-field radiation; once the phase of polarization cannot be continuously defined, nonzero integer topological charges of $q \in \mathbb{Z}$ emerge, generating polarization singularities in momentum space, at which the polarization of radiation cannot be defined, and thus the radiation itself cannot exist, which are exactly the BICs. Besides the non-Hermitian systems with open channels, BICs can also be realized in $\mathcal{PT}$-symmetric systems.

As topological invariants, topological charges are conserved and quantized quantities; they continuously evolve in momentum space and cannot suddenly disappear unless one charge drops out of the light cone or annihilates with another charge with the opposite sign. Recent experimental advances have confirmed the existence of topological charges and the topological interpretation of BICs by directly observing the polarization

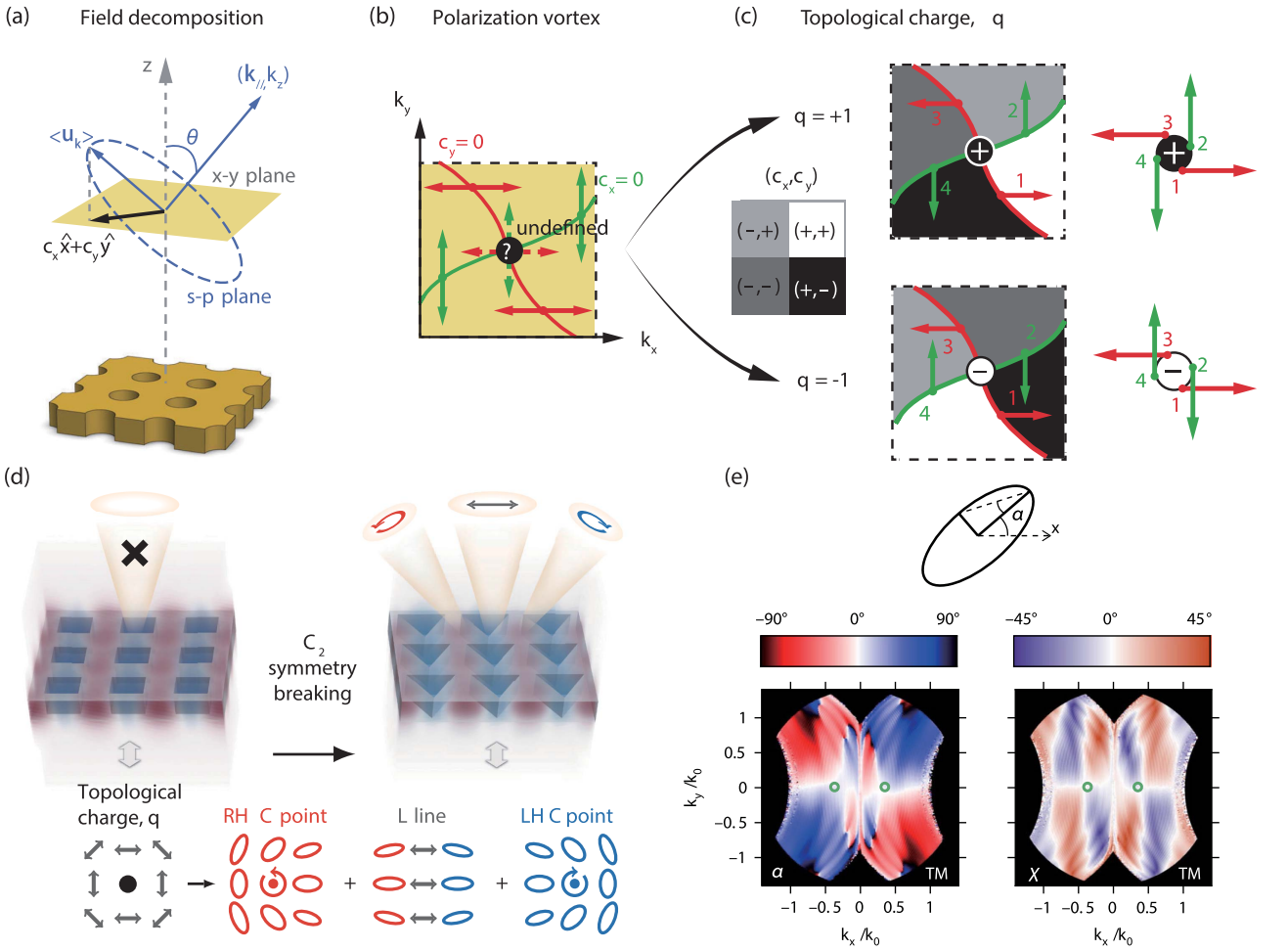

Fig. 1. Topological charges: topological nature of BICs and C-points [106,109,110]. (a) Schematic of radiation field decomposition for resonances of a PhC slab. The polarization vector (c_x, c_y) is the projection on the x–y plane of electric field $\langle u_k \rangle$ of the radiative wave. A resonance turns into a BIC if and only if $c_x = c_y = 0$. (b) Nodal lines of c_x and c_y. At the crossing point, polarization of resonance becomes undefined, where the BIC resides. (c) Two possible configurations of the polarization field near a BIC, giving rise to topological charges of $q = +1$ and $q = -1$. (d) Formation of half-integer charges carried by C-points split from an integer topological charge of a BIC. R(L)H, right (left) handed. (e) Measured polarization angles α in momentum space. A polarization vortex is visible in the map of α, denoted as green circles representing the location of BICs. Panels (a)–(c) are reproduced with permission from [106], copyright 2014 American Physical Society (APS); (d) is reproduced with permission from [110], copyright 2019 American Physical Society (APS); (e) is reproduced with permission from [109], copyright 2018 Springer Nature.

vortices [Fig. 1(e)] as well as the vanishing of Fano reflection around the vortex center [109,111]. The robustness of topological charges is also verified by annihilating a BIC state with C_2 asymmetry [110], shown in Fig. 1(d). It is found that the integer topological charge carried by the original BIC splits into a pair of half-integer charges carried by two circularly polarized (CP) states with opposite helicities, as $q = 1 = 1/2 + 1/2$. The CP states carrying half-integer topological charges are denoted as C-points.

Another unique feature of the non-Hermitian system is the EPs, at which states are completely degenerate, in both eigenvectors and eigenvalues. EPs have been widely investigated in the $\mathcal{PT}$-symmetric systems [65], at which the $\mathcal{PT}$ symmetry is spontaneously broken. It was shown that encircling an isolated EP generates a nontrivial global Berry phase [60–62,112], whose sign depends on the loop direction, showing a chiral behavior [112,113]. Recently, researchers observed the missing dimension at EPs in both photonic and acoustic wave systems [114], which comes from the reduction of geometric multiplicity due to eigenspace collapse.

EPs can be generated from conventionally degenerate points in Hermitian systems, and the energy bands around EPs have complex geometric properties. For example, in contrast to conventional cone-like dispersion, geometry of energy bands around Dirac points in the honeycomb lattice with $\mathcal{PT}$ perturbations becomes tachyon-like Riemann surfaces [115]; Dirac points are spawned into an exceptional ring full of non-isolated EPs. An exceptional ring in non-Hermitian 3D topological systems spawned from the Weyl point was also proposed [116].

In addition to the $\mathcal{PT}$ system, optical radiation in photonic systems with open channels can also result in EPs [left and middle panels, Fig. 2(a)]. It has been confirmed that, an exceptional ring can be generated from an accidental degenerate point of energy bands in 2D topologically trivial photonic systems

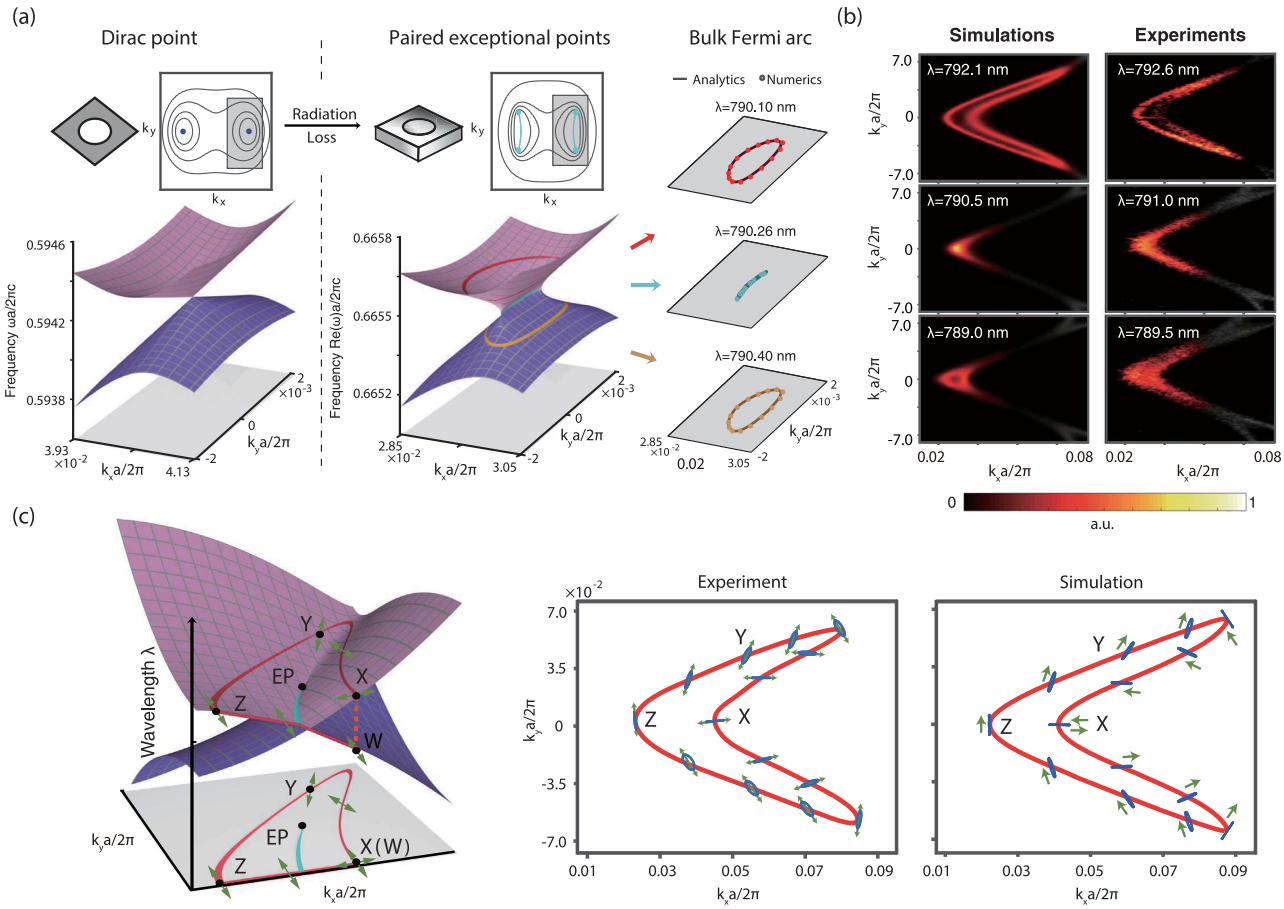

Fig. 2. Bulk Fermi arc and half-integer topological charge [93]. (a) Left: Dirac points in 2D Hermitian PhC as the accidental degeneracy under C_2 symmetry; middle: paired EPs in 2D non-Hermitian PhC slab spawn from Dirac points; right: examples of the isofrequency contours, including the open bulk Fermi arc connecting two EPs (middle panel), and closed contours at higher (upper panel) or lower (lower panel) frequencies. (b) Numerically simulated and experimentally measured isofrequency contours at three representative wavelengths. The bulk Fermi arc appears at 791.0 nm (middle panels), when the isofrequency contour becomes open-ended. (c) Experimental demonstration of the half-integer topological charges around the bulk Fermi arc. Left: schematic of polarization winding along a loop enclosing an EP; middle and right: experimental and simulated results of the polarization information along the isofrequency contour, exhibiting a half-integer topological charge of polarization vectors. Panels (a)–(c) are reproduced with permission from [93], copyright 2018 American Association for the Advancement of Science (AAAS).

under C_4 symmetry [113,117,118], giving rise to some counter-intuitive propagating properties such as zero-index materials [117,119].

Like paired Weyl points connected by a surface Fermi arc in their surface projections [120–123], paired EPs, the non-Hermitian counterparts of Weyl points, are connected by bulk Fermi arcs, corresponding to the intersections of two Riemann sheets associated with the EPs [right panel, Fig. 2(a)]. This exotic phenomenon was observed in non-Hermitian photonic systems in 2018 [93], in which a pair of isolated EPs was realized in 2D open PhC slabs with C_2 symmetry, and the bulk Fermi arcs were successfully observed from far-field radiation, as shown in Fig. 2(b). In this seminal work, it is confirmed that the radiation channel in open photonic systems provides a natural and effective way to observe and exploit the topology of energy bands.

Moreover, such work also showed that a half-integer topological charge in the polarization of far-field radiation is discovered around the bulk Fermi arc, shown in Fig. 2(c). Different from the integer topological charges associated with BICs, these half-integer topological charges are direct consequences of EPs, revealing the non-Hermitian topology of the bulk bands. It is revealed that there is an intrinsic connection between the band topology and the topology of far-field radiation. It should be emphasized that special resonant states (BICs and C-points) and nonzero Berry phases (EPs) can both be related to polarization singularities in radiation, but only the latter is topologically nontrivial upon the energy band, corresponding to nonzero Chern numbers. In former cases, the bulk wave functions are always well-defined with continuous phases except for extra degeneracies.

3. MANIPULATION RADIATION CHARACTERISTICS FROM TOPOLOGICAL CHARGES EVOLUTION

Regardless of where the topological charges originate from, they encode the geometry of the radiation field and depict the

characteristics of radiation. Therefore, their evolution in momentum space also offers the opportunity in manipulating radiation. In this section, some experimental works are introduced to give a brief summary of recent progresses in manipulation of radiation channels using topological charges. In these breakthroughs, the decay rates and directionality of the radiations are regulated through topological charge evolution in momentum space, resulting in freely controlled radiation channels to be open or closed.

A. Suppress Out-of-Plane Scattering by Merging Integer Topological Charges

The first example of manipulation on radiation channels is the merging BICs reported by Jin *et al.* [124]. Since the lifetime of BICs can be infinity in theory, they are good candidates for realizing on-chip light trapping [125–127]. However, in realistic devices, the quality (Q) factors of BICs are limited to about 1×10^4 [125], much lower than that of other high-Q resonators operating outside the continuum. The energy consumption mainly comes from the inevitable scattering losses due to random fluctuations induced by fabrication imperfections, which are the major reason resulting in Q degrading.

To address this problem, the work proposed to use a particular topology configuration to protect the high-Q resonance from out-of-plane scattering, shown in Fig. 3(a). Considering a square lattice PhC slab with nine BICs [left panel, Fig. 3(a)], each BIC is represented by polarization singularity with integer topological charge of $q = \pm 1$, respectively. Among these nine BICs, one pins at the center of the BZ (second Γ point), owing to the symmetry, while the remaining eight continuously evolve along the highly symmetric lines in momentum space, due to the conservation law of topological charges. By continuously tuning a given structural parameter, lattice periodicity a for instance, the eight off-Γ BICs keep moving and merging towards the BZ center [middle panel, Fig. 3(a)] before eventually annihilating into a single isolated BIC with a charge of $q = +1$ at Γ point [right panel, Fig. 3(a)]. This special topological configuration is named merging BICs.

The topological charge configuration determines the radiation loss of nearby resonances, and further gives rise to a bound to the scattering loss. In contrast to an isolated topological charge with the quadratic scaling rule of radiation losses (k^2, k is the momentum distance away from the charge), the topological consequence of merging BICs results in a different scaling rule of k^6, shown in Fig. 3(b). The dramatic promotion of the scaling rule from k^2 to k^6 results in an improvement of Q of resonances around the Γ point and significant suppression of the scattering losses. Therefore, merging BICs can raise the upper limit of Q factors achievable in practice. The experiment proves such theoretical findings: the highest Q observed on the merging BICs sample is 4.9×10^5 [left panel, Fig. 3(c)], 12 times higher than the isolated BIC sample fabricated on the same wafer through the same process, whose highest observed Q is about only 4.0×10^4 at the same k-point [right panel, Fig. 3(c)].

B. Realize Unidirectional Emission from Merged Half-Integer Charges

Another example of manipulating radiation is the realization of unidirectional guided resonances (UGRs) reported by Yin *et al.* [128]. Unidirectional emission is important for varieties of optoelectronic applications, since it can effectively improve the energy efficiency of those key devices, such as grating couplers [129] and PhC surface emitting lasers (PCSELs) [126].

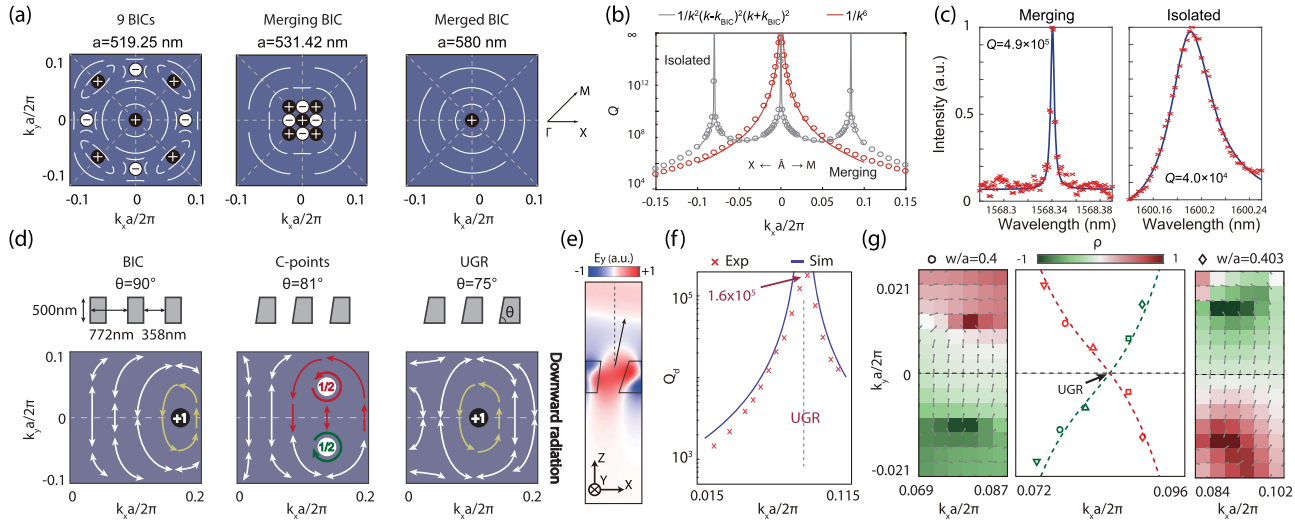

Fig. 3. Manipulation radiation characteristics from topological charges [124,128]. (a) Topological charges evolution for merging BICs. Middle panel represents the configuration of merging BICs. (b) Scaling rules of Q factors along with k-points for isolated BICs and merging BICs. (c) Experimentally measured Q factors for merging BICs (left) and isolated BICs (right) under the same fabrication process. (d) Topological charge evolution for UGRs. Charges with $q = \pm 1/2$ in the middle panel denote the C-points corresponding to CP states with opposite helicity. Right panel represents the configuration of UGRs. (e) Profile of electric field component E_y of UGR. (f) Experimental and simulated results of downward Q factors around UGR. (g) Experimentally measured trajectories of two half-integer topological charges that evolve along with the varied width of air bars of 1D PhC slab w. The crossing point of two trajectories verifies the existence of UGR. Panels (a)–(c) are reproduced with permission from [124], copyright 2019 Springer Nature; panels (d)–(g) are reproduced with permission from [128], copyright 2020 Springer Nature.

Since conventional mirrors are usually bulky, complex, dispersive, and dissipative, unidirectional emission without a mirror becomes an important feature in many scenarios [130].

Recently, it was found that unidirectional out-of-plane radiation can be realized by manipulating the evolution of topological charges, shown in Fig. 3(d). Starting from an off-Γ BIC in a 1D silicon PhC slab, it carries integer topological charges upon both upward and downward radiation [left panel, Fig. 3(d)]. Then, by tilting the sidewall, C_2 asymmetry and vertical-mirror asymmetry are induced, and the integer charges are split into paired half-integer charges protected by y-mirror symmetry on both the top/bottom sides of the slab [middle panel, Fig. 3(d)]. Since the vertical symmetry has been broken, the downward radiation channel is decoupled completely from the upward one, which means that the evolution of paired half-integer topological charges on the two sides of the slabs can be controlled independently, forming different topological configurations.

By continuously tuning the tilted angle of side walls, a particular topological configuration was realized in which the integer topological charge only exists at the downward radiation. Specifically, when gradually increasing the tilted angle, paired half-integer charges evolve in momentum space that follow different trajectories for the upward/downward radiations. For a tilted angle of 75°, the paired half-integer charges merge into an integer charge in downward radiation [right panel, Fig. 3(d)], while they keep departing from each other in upward radiation. In this way, the downward radiation channel is closed owing to integer topological charges, but the upward radiation channel remains open, thus generating a particular resonance with unidirectional emission named UGR, whose profile is shown in Fig. 3(e).

The radiation characteristics of UGRs are observed by directly measuring the asymmetric ratio $\eta = \gamma_t/\gamma_b$ between upward and downward radiation. Here, $\gamma_{t,b}$ are decay rates in upward and downward radiation channels. At the UGR, the measured asymmetric ratio is as high as 27.7 dB, equivalent to Q factor $Q_b = 1.6 \times 10^5$, which only accounts for downward radiation [Fig. 3(f)]. These results indicate 99.8% of the energy radiates through the upward channel, which exactly confirms the unidirectional emission. The evolution of topological charges was directly observed by measuring the C-points from the downward radiation [Fig. 3(g)]. The realization of UGRs is the first, to the best of our knowledge, example of closing given radiation channels from the topology perspective, which is useful for many optoelectronic devices, including light detection and ranging (LIDAR) antennas, PCSELs, and quantum cascade lasers.

4. MANIPULATING RADIATION WAVE-FRONTS FROM TOPOLOGICAL CONCEPTS

Besides manipulating the emission power and directionality of radiation, the wave-front of far-field radiation, for example, the polarizations and phase patterns, can also be manipulated from topological concepts. In this section, we focus on several recent progresses of using topological ideas in generating vortex beam—a spiral wave-front carrying nonzero orbit angular momentum (OAM) [131], which paves the way for utilizing rich DOFs of light for many applications, such as optical communication multiplexing, photonic signal processing, and superresolution microscopy.

A. Generate Vortex Beams from Topological Charges

The integer topological charges, namely the winding of polarization vectors in radiation, provide a natural and flexible way to generate vortex/vector beams in chip-scale. Years ago, vortex beams with sophisticated patterns were realized by utilizing high-order topological charges in PCSELs, in which the winding numbers of the polarization vectors are determined by the orders of the integer charges [132]. In this work, the second Γ point with different rotational symmetries (C_4 and C_6 symmetry) and the high-order Γ point (Γ_5) are employed to produce topological charges $q = 1, 2, 3$, giving rise to vortex beams with quantum numbers of OAM $l = 1, 2, 3$.

Recently, it is revealed that the ultra-fast dynamically controlled vortex beam based on microlasers can also be realized by exploiting topological charges. As reported by Huang *et al.* [133], the lasing is based on a perovskite metasurface which is fabricated from a 220 nm $MAPbBr_3$ film sandwiched by a glass substrate ($n_{sub} = 1.5$) and polymethyl methacrylate (PMMA) cladding ($n_{pmma} = 1.49$) in a square lattice spacing of 280 nm [top panel, Fig. 4(a)]. The BIC with $q = 1$ resides at the Γ point and is exhibited as a vortex. Through changing the spatial profile of pumping light from a circle to an ellipse [top panel, Fig. 4(b)], the symmetry required by the BIC breaks because the optical pumping induced gain actually corresponds to the imaginary part of the refractive index. As a result, the vortex lasing beam (a signature of BIC lasing) switches to a linearly polarized beam [bottom panel, Fig. 4(b)] or vice versa, with switching time of 1 to 1.5 ps, and the switching takes remarkably low energy consumption. The results indeed show the topological charge creates unique ultra-fast and practical useful beam manipulation.

More specifically, through changing the pumping profile spatially from a circle to an ellipse, the fourfold symmetry required by the integer topological charges is broken. As a result, the integer topological charge no longer exists, and the vortex lasing beam disappears and switches to a linearly polarized beam. Since the profile of external pumping light is flexible to control, transition from vortex lasers to linear lasers or vice versa can be realized by destroying or restoring integer topological charges through modulating the redistribution of the optical gain profile. In experiments, the fork-shaped self-interference pattern is observed to verify this vortex lasing under the circular gain profile [bottom panel, Fig. 4(a)]. When another pumping light with the same profile is overlapped with but slightly deviated from the former one, it is equivalent to an ellipse-shaped gain profile. Then, it is observed that the emission profile switched from radial donuts to two linearly polarized lobes in 1 to 1.5 ps [top panel, Fig. 4(c)]. By applying the third pumping light to recover the C_4 symmetry, the laser beam returns to vortex beam also in a few picoseconds [bottom panel, Fig. 4(c)].

It is noteworthy that, besides the lasers, passive devices are also capable of generating vortex beams. Recently, a diffraction-resistant, even-order quasi-Bessel beam has been demonstrated based on topological charges in passive PhC upon a free-standing silicon nitride slab, reported by Wang *et al.* [134].

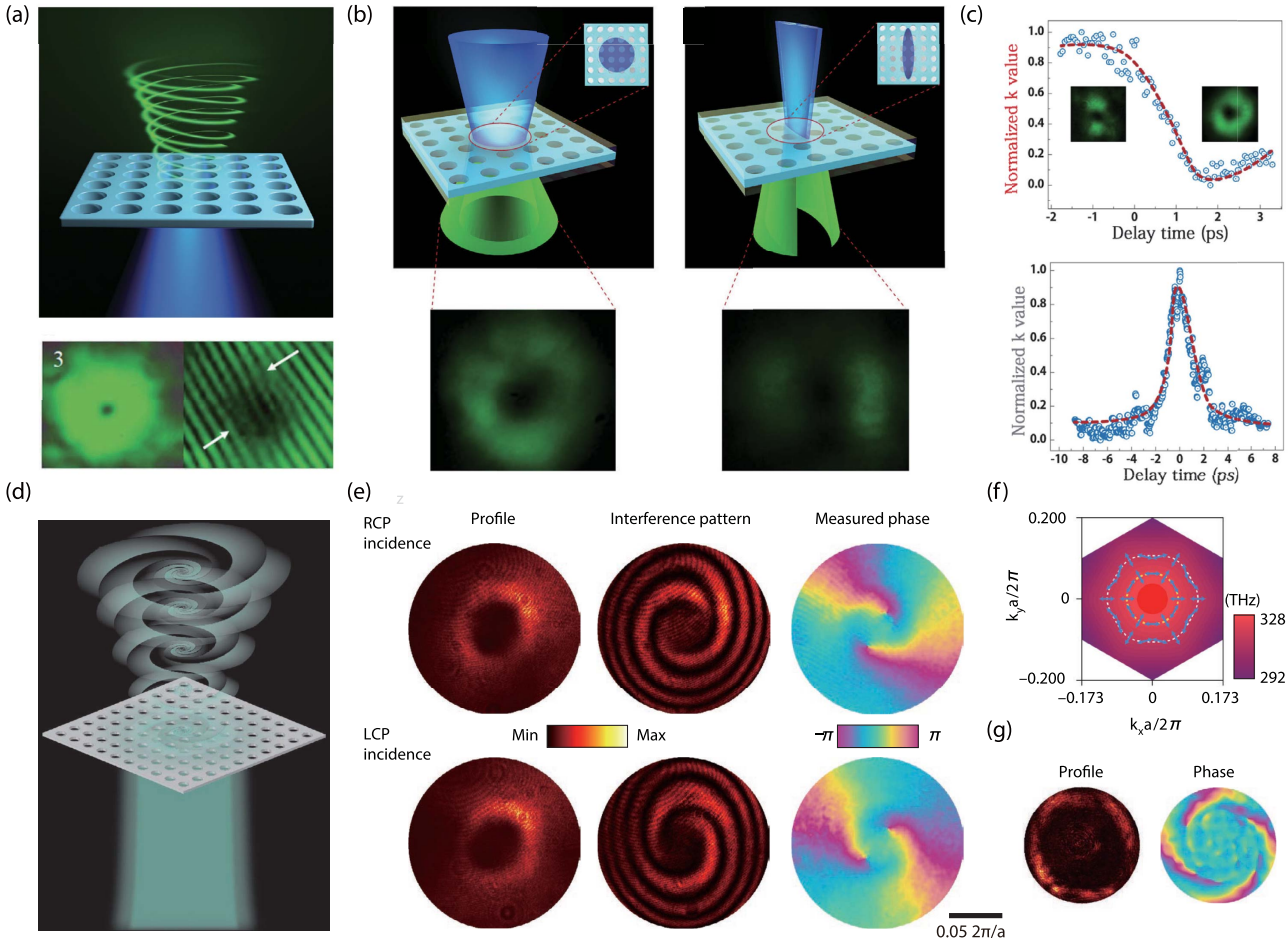

Fig. 4. Generate vortex beams based on topological charges [133,134]. (a) Top: schematic illustration of the designed perovskite metasurface pumped by laser light, generating a vortex beam based on topological charge; bottom: donut-shaped emission profile and inverted fork-shaped self-interference pattern of output vortex beam. (b) Dynamic control of output beam based on manipulating the optical gain profile. Schematics of the experiments (top) and experimentally measured emission patterns (bottom). The emission profile switches to two lobes (right panels) from the donut shape (left panels) when the profile of the pumping light is changed from a circle to an ellipse. (c) Top: transition from a donut beam to a linearly polarized two-lobe beam. Insets are corresponding emission profiles of the output beam; bottom: transition from a donut beam to a two-lobe beam and back, within a picosecond-scale transition time. (d) Schematic illustration of a passive vortex beam generator based on a PhC slab. (e) Far-field patterns and interferograms of output beams under different incident polarization. (f) Polarization winding of topological charge $q = -2$. (g) Vortex beam with OAM of $l = 4$ based on topological charge of $q = -2$. Panels (a)–(c) are reproduced with permission from [133], copyright 2020 AAAS; panels (d)–(g) are reproduced with permission from [134], copyright 2020 Springer Nature.

By applying a CP incident beam to the PhC slab with integer topological charges q, the output vortex beam with OAM of $l = \mp 2q$ is obtained, shown in Fig. 4(d). Owing to the conservation law of topological charges, the OAM carried by the output beam is completely determined by the topological charges of incidence and optical resonance [Fig. 4(e)]. Therefore, the output OAM can be switched by changing the wavelength of incidence that selectively couples to different orders of Γ points, at which their topological charges q are different [Fig. 4(f)].

B. Generate Vortex Beams from Spin-Momentum Locking

In spite of the topological charges upon radiation polarization vectors, tunable vortex beams can also be realized based on other topological concepts, i.e., spin-orbit locking. In work reported by Yang *et al.*, a microlaser working at a topologically protected edge state with spin-momentum locking is employed to help an out-of-plane vortex beam emerge in a non-Hermitian PhC slab [135].

Specifically, the work starts from a honeycomb lattice, with doubly degenerate Dirac cones at the Γ point. By deforming the honeycomb lattice into a triangular lattice with hexagonal clusters of six neighboring sites, the degeneracy of the two Dirac cones is lifted, opening a topologically nontrivial bandgap around the Γ point. As an optical analog of QSHE, two Dirac cones at the Γ point in such a triangle lattice correspond to spin-up and spin-down states as pseudo-TR pairs due to different in-plane symmetries [136]. Therefore, a photonic Z2 insulator was realized in such a lattice with topologically nontrivial interface between two PhC domains, which are distinct in topology but share a common bulk bandgap [bottom

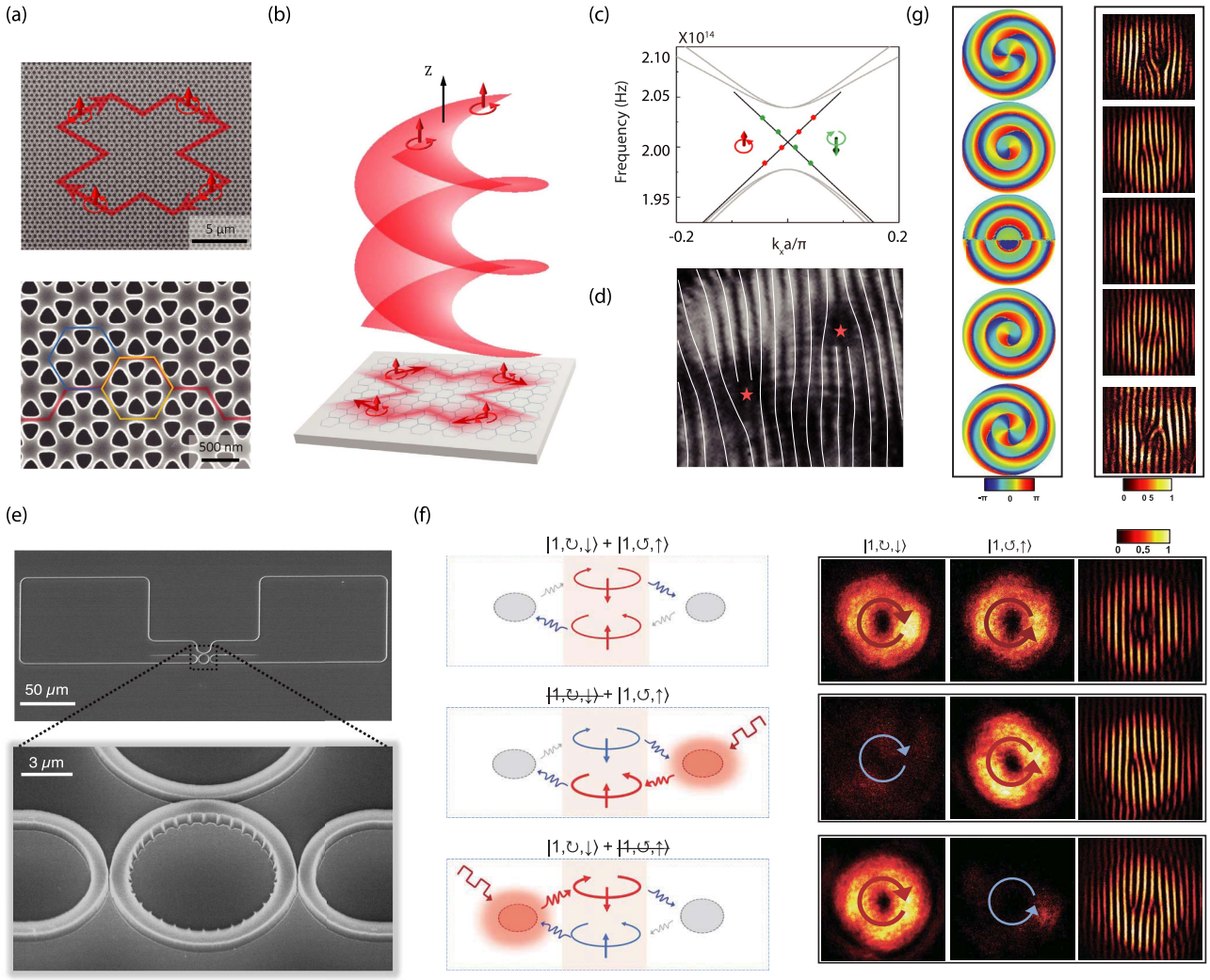

Fig. 5. Generate vortex beams based on spin-momentum locking [135,137]. (a) Top: scanning electron microscope (SEM) image of a topological vortex laser with an X-shaped PhC cavity (red lines). The corresponding spin direction of the cavity mode is indicated by the arrows. Bottom: zoomed-in SEM image of the topological interface. Red line, topological interface; blue hexagon, unit cell in the topological PhC; orange hexagon, unit cell in the trivial PhC. (b) Schematic illustration of angular-momentum conservation of the CP vortex beam with respect to the spin-momentum-locking edge states. (c) Energy band structure of the discrete edge states (red and green dots) with surrounding bulk bands (gray lines). Red dots, spin-up edge states; green dots, spin-down edge states. (d) Pattern of self-interference of the output beam, verifying OAM of $l = -2$. (e) SEM images of the vortex beam generator based on WGMs in the ring resonator. (f) Non-Hermitian interactions and corresponding emission pattern. Top panels: without non-Hermitian interactions, no phase winding exists in the output beam; middle and bottom panels: with unidirectional non-Hermitian interaction, the self-interference pattern exhibits an inverted fork shape, verifying the vortex beam. (g) Five channels of different OAMs are realized in microlasers shown in (e). Panels (a)–(c) are reproduced with permission from [133], copyright 2020 American Physical Society (APS); panels (d)–(g) are reproduced with permission from [134], copyright 2020 AAAS.

panel, Fig. 5(a)]. Inside the bandgap, paired helical edge states appear with spin-momentum locking, namely that the edge states with different spins would propagate in opposite directions.

Further, an X-shaped laser cavity is demonstrated by using such a topological interface, shown in the top panel of Fig. 5(a). Due to the finite cavity size, the paired edge states allowed inside the bandgap become discrete in the energy band, with different quantized quantum numbers of OAM l [top panel, Fig. 5(c)]. In this way, each pair of edge states can be denoted as $|l, \sigma\rangle$, in which σ denotes the spin angular momentum (SAM), with two quantum numbers of spin-up (+) and spin-down (–). Clearly, the signs of the spin and OAM are locked due to spin-momentum locking.

Different from the conventional edge states around Dirac cones at K and K' points under the light cone, here the edge states reside around the Γ point that is embedded in the light cone, which implies that the edge states are intrinsically radiative into the continuum and can be probed via far-field radiation, shown in Fig. 5(b). The circular polarization and OAM of the radiation beam thus correspond to the pseudo-spin and OAM of the edge modes owing to angular-momentum

conservation. Because of the protection of pseudo-TR symmetry, two edge states are completely decoupled from each other. By designing the pumping light, only one edge state can be chosen to lase. The bottom panel of Fig. 5(c) gives the radiation features of the lasing edge mode $|-2,+\rangle$. The emission profile shown in Fig. 5(d) exhibits a donut shape, and the self-interference patterns are fork-shaped, indicating a vortex beam with OAM of $l=-2$. Lasing of the TR counterpart $|2,-\rangle$ definitely gives rise to a vortex beam with OAM of $l=2$.

Another work reported by Zhang *et al.* demonstrated a tunable topological charge vortex microlaser on spin-orbit locking WGMs [137]. As shown in Fig. 5(e), a microlaser system consists of a microring resonator that is coupled to a waveguide with two control arms. By tuning the geometry of the waveguide, spin-orbit interaction is manipulated and consequently couples the right-hand (spin-down: ↓) and left-hand (spin-up: ↑) circular polarizations with the clockwise (CW, ↻) and CCW (↺) modes, respectively [Fig. 5(f)]. ↺ and ↻ denote the signs of OAM. The spin-orbit-locking WGMs are denoted as $||l|,\circlearrowleft,\uparrow\rangle$ and $||l|,\circlearrowright,\downarrow\rangle$, in which the quantum number l refers to the OAM of output emission.

In order to extract the OAM into the far-field radiation, periodic angular scatters on the inner sidewalls are designed to make WGMs radiative. Therefore, the order of WGM itself N and the number of scatters M together determine the total conserved angular momentum $J=\mathrm{sgn}(\sigma)(N-M)$, where σ is the quantum number of SAM. For appropriately designed scatters, a total angular momentum of $|J|=2$ is achieved, consisting of an SAM of $|\sigma|=1$ and OAM of $|l|=1$.

In the absence of non-Hermitian interaction, two spin-orbit-locking WGMs are degenerate. When they lase simultaneously, no notable phase-discontinuity was observed in the off-center self-interference pattern, indicating no phase winding in the output beam [top panels, Fig. 5(f)]. By contrast, unidirectional non-Hermitian coupling is applied by selectively pumping one control arm, which breaks the helical symmetry and the degeneracy of WGMs. As a result, only one chiral WGM state is pumped to lase, and the other is suppressed. The patterns of far-field emission and self-interference pattern are shown in the middle panels of Fig. 5(f), when the right control arm is illuminated. An interference pattern of paired inverted forks verifies the OAM of $l=1$. Similarly, when the left control arm is selectively pumped, the orientation of the fork shape is reversed, indicating an OAM of $l=-1$ [bottom panels, Fig. 5(f)].

Moreover, the dynamic reconfiguration of OAM was also demonstrated in this vortex beam generator. By applying a movable radial polarizer to filter out the lasing light, the beam is transferred from CP to linear polarization, and thus the SAM is tuned to zero accordingly. Since the total angular momentum must be conserved, the lasing state is switched from $|l=\pm1,\sigma=\pm1\rangle$ to $|l=\pm2,\sigma=0\rangle$, and high-order OAMs are achieved. As a result, this reconfigurable vortex microlaser provides five channels of different OAMs in the range of $l=\pm2,\pm1,0$, and all of these OAM states work at the same wavelength, shown in Fig. 5(g). Similar to the work mentioned above, the switching time is, in principle, restricted by the optical response time of semiconductor material, which could be potentially in the picosecond scale.

5. SUMMARY AND OUTLOOK

Non-Hermitian topology is a rapidly emerging field with growing literature and progress through the effort of the entire research community, including new phenomena, theories, methods, and applications, ranging from fundamental understanding of the roles of gain/loss, manipulating the radiations, to the novel devices for vortex beam generation, and others. More future possibilities and advances are expected as well.

From the view of science, it is essential to build up a comprehensive theoretical framework for non-Hermitian topology. Given that many anomalous phenomena in a variety of non-Hermitian systems were discovered and explained from different theoretical treatments, a lack of unified and consistent theories of non-Hermicity, in particular how the radiation raises and represents unique topology landscapes, is still an obstacle preventing deeper understanding of the physics and realizing of practical applications. For instance, both the BICs and EPs carry topological charges in their far-field radiation, but only the latter ones are associated with nontrivial Chern numbers. Therefore, an interconnection between the band topology and the topology upon the radiation is still waiting for exploration. Besides, from the view of technology, high-order topological charges that reside at high-order Γ points or higher crystalline symmetries other than C_4 symmetry may have much potential in bringing more DOFs for manipulating the radiation and boosting the applications such as ultra-high-Q cavities, ultra-sensitive sensors, and multi-channel OAM multiplexing.

To sum up, since the radiation channels allow the light in and out, there is no doubt that the radiation will bring fundamental differences and extra DOFs from topological perspectives compared to its Hermitian counterparts, while, at the same time, offering a natural channel for probing and exploiting the intrinsic band topology. In this review, we have summarized a part of new phenomena corresponding to the interplay between the non-Hermiticity and topology and emphasized several breakthroughs in manipulating radiation from the perspective of topological concepts. We believe that further collision and merging between conventional topological concepts and non-Hermiticity will inspire new ideas in utilizing topological properties for photonic and optoelectronic applications.

Funding. National Natural Science Foundation of China (61922004).

Disclosures. The authors declare no conflicts of interest.

REFERENCES

1. L. Lu, J. D. Joannopoulos, and M. Soljačić, "Topological photonics," Nat. Photonics **8**, 821–829 (2014).
2. A. B. Khanikaev and G. Shvets, "Two-dimensional topological photonics," Nat. Photonics **11**, 763–773 (2017).
3. T. Ozawa, H. M. Price, A. Amo, N. Goldman, M. Hafezi, L. Lu, M. C. Rechtsman, D. Schuster, J. Simon, O. Zilberberg, and I. Carusotto, "Topological photonics," Rev. Mod. Phys. **91**, 015006 (2019).

4. H. Wang, S. K. Gupta, B. Xie, and M. Lu, "Topological photonic crystals: a review," Front. Optoelectron. **13**, 50–72 (2020).
5. Z. Wang, Y. Chong, J. D. Joannopoulos, and M. Soljačić, "Observation of unidirectional backscattering-immune topological electromagnetic states," Nature **461**, 772–775 (2009).
6. M. Hafezi, S. Mittal, J. Fan, A. Migdall, and J. M. Taylor, "Imaging topological edge states in silicon photonics," Nat. Photonics **7**, 1001–1005 (2013).
7. M. Hafezi, E. A. Demler, M. D. Lukin, and J. M. Taylor, "Robust optical delay lines with topological protection," Nat. Phys. **7**, 907–912 (2011).
8. K. Lai, T. Ma, X. Bo, S. Anlage, and G. Shvets, "Experimental realization of a reflections-free compact delay line based on a photonic topological insulator," Sci. Rep. **6**, 28453 (2016).
9. A. Kodigala, T. Lepetit, Q. Gu, B. Bahari, Y. Fainman, and B. Kante, "Lasing action from photonic bound states in continuum," Nature **541**, 196–199 (2017).
10. Z.-K. Shao, H.-Z. Chen, S. Wang, X.-R. Mao, Z.-Q. Yang, S.-L. Wang, X.-X. Wang, X. Hu, and R.-M. Ma, "A high-performance topological bulk laser based on band-inversion-induced reflection," Nat. Nanotechnol. **15**, 67–72 (2020).
11. Y. Zeng, U. Chattopadhyay, B. Zhu, B. Qiang, J. Li, Y. Jin, L. Li, A. G. Davies, E. H. Linfield, B. Zhang, Y. Chong, and Q. J. Wang, "Electrically pumped topological laser with valley edge modes," Nature **578**, 246–250 (2020).
12. K. V. Klitzing, G. Dorda, and M. Pepper, "New method for high-accuracy determination of the fine-structure constant based on quantized Hall resistance," Phys. Rev. Lett. **45**, 494–497 (1980).
13. D. J. Thouless, M. Kohmoto, M. P. Nightingale, and M. den Nijs, "Quantized Hall conductance in a two-dimensional periodic potential," Phys. Rev. Lett. **49**, 405–408 (1982).
14. M. Z. Hasan and C. L. Kane, "Colloquium: topological insulators," Rev. Mod. Phys. **82**, 3045–3067 (2010).
15. J. E. Moore, "The birth of topological insulators," Nature **464**, 194–198 (2010).
16. Y. Hatsugai, "Chern number and edge states in the integer quantum Hall effect," Phys. Rev. Lett. **71**, 3697–3700 (1993).
17. Y. Hatsugai, "Edge states in the integer quantum Hall effect and the Riemann surface of the Bloch function," Phys. Rev. B **48**, 11851–11862 (1993).
18. X.-L. Qi, Y.-S. Wu, and S.-C. Zhang, "General theorem relating the bulk topological number to edge states in two-dimensional insulators," Phys. Rev. B **74**, 045125 (2006).
19. C. L. Kane and E. J. Mele, "Quantum spin Hall effect in graphene," Phys. Rev. Lett. **95**, 226801 (2005).
20. C. L. Kane and E. J. Mele, "Z2 topological order and the quantum spin Hall effect," Phys. Rev. Lett. **95**, 146802 (2005).
21. B. A. Bernevig and S.-C. Zhang, "Quantum spin Hall effect," Phys. Rev. Lett. **96**, 106802 (2006).
22. J. E. Moore and L. Balents, "Topological invariants of time-reversal-invariant band structures," Phys. Rev. B **75**, 121306 (2007).
23. L. Fu and C. L. Kane, "Topological insulators with inversion symmetry," Phys. Rev. B **76**, 045302 (2007).
24. L. Fu, C. L. Kane, and E. J. Mele, "Topological insulators in three dimensions," Phys. Rev. Lett. **98**, 106803 (2007).
25. B. A. Bernevig, T. L. Hughes, and S.-C. Zhang, "Quantum spin Hall effect and topological phase transition in HgTe quantum wells," Science **314**, 1757–1761 (2006).
26. D. Hsieh, D. Qian, L. Wray, Y. Xia, Y. S. Hor, R. J. Cava, and M. Z. Hasan, "A topological Dirac insulator in a quantum spin Hall phase," Nature **452**, 970–974 (2008).
27. H. Zhang, C.-X. Liu, X.-L. Qi, X. Dai, Z. Fang, and S.-C. Zhang, "Topological insulators in Bi_2Se_3, Bi_2Te_3 and Sb_2Te_3 with a single Dirac cone on the surface," Nat. Phys. **5**, 438–442 (2009).
28. Y. L. Chen, J. G. Analytis, J.-H. Chu, Z. K. Liu, S.-K. Mo, X. L. Qi, H. J. Zhang, D. H. Lu, X. Dai, Z. Fang, S. C. Zhang, I. R. Fisher, Z. Hussain, and Z.-X. Shen, "Experimental realization of a three-dimensional topological insulator, Bi_2Te_3," Science **325**, 178–181 (2009).
29. M. König, S. Wiedmann, C. Brüne, A. Roth, H. Buhmann, L. W. Molenkamp, X.-L. Qi, and S.-C. Zhang, "Quantum spin Hall insulator state in HGTE quantum wells," Science **318**, 766–770 (2007).
30. M. Ezawa, "Symmetry protected topological charge in symmetry broken phase: spin-Chern, spin-valley-Chern and mirror-Chern numbers," Phys. Lett. A **378**, 1180–1184 (2014).
31. A. F. Morpurgo and F. Guinea, "Intervalley scattering, long-range disorder, and effective time-reversal symmetry breaking in graphene," Phys. Rev. Lett. **97**, 196804 (2006).
32. A. Rycerz, J. Tworzydlo, and C. W. J. Beenakker, "Valley filter and valley valve in graphene," Nat. Phys. **3**, 172–175 (2007).
33. L. Ju, Z. Shi, N. Nair, Y. Lv, C. Jin, J. Velasco, C. Ojeda-Aristizabal, H. A. Bechtel, M. C. Martin, A. Zettl, J. Analytis, and F. Wang, "Topological valley transport at bilayer graphene domain walls," Nature **520**, 650–655 (2015).
34. T. Ma and G. Shvets, "All-Si valley-Hall photonic topological insulator," New J. Phys. **18**, 025012 (2016).
35. J. Noh, S. Huang, K. P. Chen, and M. C. Rechtsman, "Observation of photonic topological valley Hall edge states," Phys. Rev. Lett. **120**, 063902 (2018).
36. F. Gao, H. Xue, Z. Yang, K. Lai, Y. Yu, X. Lin, Y. Chong, G. Shvets, and B. Zhang, "Topologically protected refraction of robust kink states in valley photonic crystals," Nat. Phys. **14**, 140–144 (2018).
37. M. Ezawa, "Spin valleytronics in silicene: quantum spin Hall-quantum anomalous Hall insulators and single-valley semimetals," Phys. Rev. B **87**, 155415 (2013).
38. J.-W. Dong, X.-D. Chen, H. Zhu, Y. Wang, and X. Zhang, "Valley photonic crystals for control of spin and topology," Nat. Mater. **16**, 298–302 (2017).
39. S. Ryu and Y. Hatsugai, "Topological origin of zero-energy edge states in particle-hole symmetric systems," Phys. Rev. Lett. **89**, 077002 (2002).
40. J. Zak, "Berry's phase for energy bands in solids," Phys. Rev. Lett. **62**, 2747–2750 (1989).
41. W. P. Su, J. R. Schrieffer, and A. J. Heeger, "Solitons in polyacetylene," Phys. Rev. Lett. **42**, 1698–1701 (1979).
42. J. C. Y. Teo, L. Fu, and C. L. Kane, "Surface states and topological invariants in three-dimensional topological insulators: application to $Bi_{1-x}Sb_x$," Phys. Rev. B **78**, 045426 (2008).
43. R. Takahashi and S. Murakami, "Gapless interface states between topological insulators with opposite Dirac velocities," Phys. Rev. Lett. **107**, 166805 (2011).
44. T. H. Hsieh, H. Lin, J. Liu, W. Duan, A. Bansil, and L. Fu, "Topological crystalline insulators in the SnTe material class," Nat. Commun. **3**, 982 (2012).
45. L. Fu, "Topological crystalline insulators," Phys. Rev. Lett. **106**, 106802 (2011).
46. F. D. M. Haldane and S. Raghu, "Possible realization of directional optical waveguides in photonic crystals with broken time-reversal symmetry," Phys. Rev. Lett. **100**, 013904 (2008).
47. M. Sato, K. Hasebe, K. Esaki, and M. Kohmoto, "Time-reversal symmetry in non-Hermitian systems," Progr. Theoret. Phys. **127**, 937–974 (2012).
48. K. Esaki, M. Sato, K. Hasebe, and M. Kohmoto, "Edge states and topological phases in non-Hermitian systems," Phys. Rev. B **84**, 205128 (2011).
49. F. Gao, Z. Gao, X. Shi, Z. Yang, X. Lin, H. Xu, J. D. Joannopoulos, M. Soljačić, H. Chen, L. Lu, Y. Chong, and B. Zhang, "Probing topological protection using a designer surface plasmon structure," Nat. Commun. **7**, 11619 (2016).
50. V. M. Martinez Alvarez, J. E. Barrios Vargas, M. Berdakin, and L. E. F. Torres, "Topological states of non-Hermitian systems," Eur. Phys. J. Spec. Top. **227**, 1295–1308 (2018).
51. H. Shen, B. Zhen, and L. Fu, "Topological band theory for non-Hermitian Hamiltonians," Phys. Rev. Lett. **120**, 146402 (2018).
52. T. Kato, *Perturbation Theory in a Finite-Dimensional Space* (Springer, 1995), pp. 62–126.
53. K. Kawabata, T. Bessho, and M. Sato, "Classification of exceptional points and non-Hermitian topological semimetals," Phys. Rev. Lett. **123**, 066405 (2019).
54. B. Peng, Å. K. Özdemir, M. Liertzer, W. Chen, J. Kramer, H. Yılmaz, J. Wiersig, S. Rotter, and L. Yang, "Chiral modes and directional

lasing at exceptional points," Proc. Natl. Acad. Sci. USA **113**, 6845–6850 (2016).
55. A. H. C. Neto, F. Guinea, N. M. R. Peres, K. S. Novoselov, and A. K. Geim, "The electronic properties of graphene," Rev. Mod. Phys. **81**, 109–162 (2009).
56. S. M. Young, S. Zaheer, J. C. Y. Teo, C. L. Kane, E. J. Mele, and A. M. Rappe, "Dirac semimetal in three dimensions," Phys. Rev. Lett. **108**, 140405 (2012).
57. X. Wan, A. M. Turner, A. Vishwanath, and S. Y. Savrasov, "Topological semimetal and Fermi-arc surface states in the electronic structure of pyrochlore iriyears," Phys. Rev. B **83**, 205101 (2011).
58. A. A. Burkov and L. Balents, "Weyl semimetal in a topological insulator multilayer," Phys. Rev. Lett. **107**, 127205 (2011).
59. L. Lu, L. Fu, J. D. Joannopoulos, and M. Soljačić, "Weyl points and line nodes in gyroid photonic crystals," Nat. Photonics **7**, 294–299 (2013).
60. M. V. Berry, "Quantal phase factors accompanying adiabatic changes," Proc. R. Soc. London A **392**, 45–57 (1984).
61. A. A. Mailybaev, O. N. Kirillov, and A. P. Seyranian, "Geometric phase around exceptional points," Phys. Rev. A **72**, 014104 (2005).
62. S.-D. Liang and G.-Y. Huang, "Topological invariance and global Berry phase in non-Hermitian systems," Phys. Rev. A **87**, 012118 (2013).
63. L. Feng, R. El-Ganainy, and L. Ge, "Non-Hermitian photonics based on parity-time symmetry," Nat. Photonics **11**, 752–762 (2017).
64. R. El-Ganainy, K. G. Makris, M. Khajavikhan, Z. H. Musslimani, S. Rotter, and D. N. Christodoulides, "Non-Hermitian physics and PT symmetry," Nat. Phys. **14**, 11–19 (2018).
65. S. K. Ozdemir, S. Rotter, F. Nori, and L. Yang, "Parity-time symmetry and exceptional points in photonics," Nat. Mater. **18**, 783–798 (2019).
66. D. Leykam, K. Y. Bliokh, C. Huang, Y. D. Chong, and F. Nori, "Edge modes, degeneracies, and topological numbers in non-Hermitian systems," Phys. Rev. Lett. **118**, 040401 (2017).
67. T. E. Lee, "Anomalous edge state in a non-Hermitian lattice," Phys. Rev. Lett. **116**, 133903 (2016).
68. S. Lin, L. Jin, and Z. Song, "Symmetry protected topological phases characterized by isolated exceptional points," Phys. Rev. B **99**, 165148 (2019).
69. A. Mostafazadeh and H. Mehri-Dehnavi, "Spectral singularities, biorthonormal systems and a two-parameter family of complex point interactions," J. Phys. A **42**, 125303 (2009).
70. A. Mostafazadeh, "Spectral singularities of complex scattering potentials and infinite reflection and transmission coefficients at real energies," Phys. Rev. Lett. **102**, 220402 (2009).
71. P. Wang, L. Jin, G. Zhang, and Z. Song, "Wave emission and absorption at spectral singularities," Phys. Rev. A **94**, 053834 (2016).
72. L. Jin and Z. Song, "Incident direction independent wave propagation and unidirectional lasing," Phys. Rev. Lett. **121**, 073901 (2018).
73. S. Yao and Z. Wang, "Edge states and topological invariants of non-Hermitian systems," Phys. Rev. Lett. **121**, 086803 (2018).
74. S. Yao, F. Song, and Z. Wang, "Non-Hermitian Chern bands," Phys. Rev. Lett. **121**, 136802 (2018).
75. F. Song, S. Yao, and Z. Wang, "Non-Hermitian skin effect and chiral damping in open quantum systems," Phys. Rev. Lett. **123**, 170401 (2019).
76. C. H. Lee and R. Thomale, "Anatomy of skin modes and topology in non-Hermitian systems," Phys. Rev. B **99**, 201103 (2019).
77. N. Okuma, K. Kawabata, K. Shiozaki, and M. Sato, "Topological origin of non-Hermitian skin effects," Phys. Rev. Lett. **124**, 086801 (2020).
78. V. M. Martinez Alvarez, J. E. B. Vargas, and L. E. F. Torres, "Non-Hermitian robust edge states in one dimension: anomalous localization and eigenspace condensation at exceptional points," Phys. Rev. B **97**, 121401 (2018).
79. F. K. Kunst, E. Edvardsson, J. C. Budich, and E. J. Bergholtz, "Biorthogonal bulk-boundary correspondence in non-Hermitian systems," Phys. Rev. Lett. **121**, 026808 (2018).
80. L. Jin and Z. Song, "Bulk-boundary correspondence in a non-Hermitian system in one dimension with chiral inversion symmetry," Phys. Rev. B **99**, 081103 (2019).
81. K. Yokomizo and S. Murakami, "Non-Bloch band theory of non-Hermitian systems," Phys. Rev. Lett. **123**, 066404 (2019).
82. F. Song, S. Yao, and Z. Wang, "Non-Hermitian topological invariants in real space," Phys. Rev. Lett. **123**, 246801 (2019).
83. A. Ghatak and T. Das, "New topological invariants in non-Hermitian systems," J. Phys. Condens. Matter **31**, 263001 (2019).
84. K. Kawabata, K. Shiozaki, M. Ueda, and M. Sato, "Symmetry and topology in non-Hermitian physics," Phys. Rev. X **9**, 041015 (2019).
85. C. Yin, H. Jiang, L. Li, R. Lü, and S. Chen, "Geometrical meaning of winding number and its characterization of topological phases in one-dimensional chiral non-Hermitian systems," Phys. Rev. A **97**, 052115 (2018).
86. H. Zhou and J. Y. Lee, "Periodic table for topological bands with non-Hermitian symmetries," Phys. Rev. B **99**, 235112 (2019).
87. L. Xiao, T. Deng, K. Wang, G. Zhu, Z. Wang, W. Yi, and P. Xue, "Non-Hermitian bulk-boundary correspondence in quantum dynamics," Nat. Phys. **16**, 761–766 (2020).
88. S. Weidemann, M. Kremer, T. Helbig, T. Hofmann, A. Stegmaier, M. Greiter, R. Thomale, and A. Szameit, "Topological funneling of light," Science **368**, 311–314 (2020).
89. J. von Neuman and E. Wigner, "Uber merkwurdige diskrete Eigenwerte. Uber das Verhalten von eigenwerten bei adiabatischen prozessen," Phys. Z. **30**, 467–470 (1929).
90. H. Friedrich and D. Wintgen, "Interfering resonances and bound states in the continuum," Phys. Rev. A **32**, 3231–3242 (1985).
91. C. W. Hsu, B. Zhen, A. D. Stone, J. D. Joannopoulos, and M. Soljačić, "Bound states in the continuum," Nat. Rev. Mater. **1**, 16048 (2016).
92. N. D. Mermin, "The topological theory of defects in ordered media," Rev. Mod. Phys. **51**, 591–648 (1979).
93. H. Zhou, C. Peng, Y. Yoon, C. W. Hsu, K. A. Nelson, L. Fu, J. D. Joannopoulos, M. Soljačić, and B. Zhen, "Observation of bulk Fermi arc and polarization half charge from paired exceptional points," Science **359**, 1009–1012 (2018).
94. D. C. Tsui, H. L. Stormer, and A. C. Gossard, "Two-dimensional magneto transport in the extreme quantum limit," Phys. Rev. Lett. **48**, 1559–1562 (1982).
95. S.-Y. Xu, I. Belopolski, N. Alidoust, M. Neupane, G. Bian, C. Zhang, R. Sankar, G. Chang, Z. Yuan, C.-C. Lee, S.-M. Huang, H. Zheng, J. Ma, D. S. Sanchez, B. Wang, A. Bansil, F. Chou, P. P. Shibayev, H. Lin, S. Jia, and M. Z. Hasan, "Discovery of a Weyl fermion semimetal and topological Fermi arcs," Science **349**, 613–617 (2015).
96. L. Lu, Z. Wang, D. Ye, L. Ran, L. Fu, J. D. Joannopoulos, and M. Soljačić, "Experimental observation of Weyl points," Science **349**, 622–624 (2015).
97. S.-C. Zhang and J. Hu, "A four-dimensional generalization of the quantum Hall effect," Science **294**, 823–828 (2001).
98. Y. E. Kraus, Z. Ringel, and O. Zilberberg, "Four-dimensional quantum Hall effect in a two-dimensional quasicrystal," Phys. Rev. Lett. **111**, 226401 (2013).
99. S. John, "Strong localization of photons in certain disordered dielectric superlattices," Phys. Rev. Lett. **58**, 2486–2489 (1987).
100. E. Yablonovitch, "Inhibited spontaneous emission in solid-state physics and electronics," Phys. Rev. Lett. **58**, 2059–2062 (1987).
101. S. Fan and J. D. Joannopoulos, "Analysis of guided resonances in photonic crystal slabs," Phys. Rev. B **65**, 235112 (2002).
102. L. Ni, Z. Wang, C. Peng, and Z. Li, "Tunable optical bound states in the continuum beyond in-plane symmetry protection," Phys. Rev. B **94**, 245148 (2016).
103. Y. Yang, C. Peng, Y. Liang, Z. Li, and S. Noda, "Analytical perspective for bound states in the continuum in photonic crystal slabs," Phys. Rev. Lett. **113**, 037401 (2014).
104. W. Chen, Y. Chen, and W. Liu, "Singularities and Poincaré indices of electromagnetic multipoles," Phys. Rev. Lett. **122**, 153907 (2019).
105. Z. Sadrieva, K. Frizyuk, M. Petrov, Y. Kivshar, and A. Bogdanov, "Multipolar origin of bound states in the continuum," Phys. Rev. B **100**, 115303 (2019).

106. B. Zhen, C. W. Hsu, L. Lu, A. D. Stone, and M. Soljačić, "Topological nature of optical bound states in the continuum," Phys. Rev. Lett. **113**, 257401 (2014).
107. E. N. Bulgakov and D. N. Maksimov, "Topological bound states in the continuum in arrays of dielectric spheres," Phys. Rev. Lett. **118**, 267401 (2017).
108. G. J. Gbur, *Singular Optics* (CRC Press, 2016).
109. H. M. Doeleman, F. Monticone, W. den Hollander, A. Alã, and A. F. Koenderink, "Experimental observation of a polarization vortex at an optical bound state in the continuum," Nat. Photonics **12**, 397–401 (2018).
110. W. Liu, B. Wang, Y. Zhang, J. Wang, M. Zhao, F. Guan, X. Liu, L. Shi, and J. Zi, "Circularly polarized states spawning from bound states in the continuum," Phys. Rev. Lett. **123**, 116104 (2019).
111. Y. Zhang, A. Chen, W. Liu, C. W. Hsu, B. Wang, F. Guan, X. Liu, L. Shi, L. Lu, and J. Zi, "Observation of polarization vortices in momentum space," Phys. Rev. Lett. **120**, 186103 (2018).
112. J. Mei, Y. Wu, C. T. Chan, and Z.-Q. Zhang, "First-principles study of Dirac and Dirac-like cones in phononic and photonic crystals," Phys. Rev. B **86**, 035141 (2012).
113. X. Yin, Y. Liang, L. Ni, Z. Wang, C. Peng, and Z. Li, "Analytical study of mode degeneracy in non-Hermitian photonic crystals with TM-like polarization," Phys. Rev. B **96**, 075111 (2017).
114. H.-Z. Chen, T. Liu, H.-Y. Luan, R.-J. Liu, X.-Y. Wang, X.-F. Zhu, Y.-B. Li, Z.-M. Gu, S.-J. Liang, H. Gao, L. Lu, L. Ge, S. Zhang, J. Zhu, and R.-M. Ma, "Revealing the missing dimension at an exceptional point," Nat. Phys. **16**, 571–578 (2020).
115. A. Szameit, M. C. Rechtsman, O. Bahat-Treidel, and M. Segev, "PT-symmetry in honeycomb photonic lattices," Phys. Rev. A **84**, 021806 (2011).
116. Y. Xu, S.-T. Wang, and L.-M. Duan, "Weyl exceptional rings in a three-dimensional dissipative cold atomic gas," Phys. Rev. Lett. **118**, 045701 (2017).
117. X. Huang, Y. Lai, Z. H. Hang, H. Zheng, and C. T. Chan, "Dirac cones induced by accidental degeneracy in photonic crystals and zero-refractive-index materials," Nat. Mater. **10**, 582–586 (2011).
118. B. Zhen, C. W. Hsu, Y. Igarashi, L. Lu, I. Kaminer, A. Pick, S.-L. Chua, J. D. Joannopoulos, and M. Soljačić, "Spawning rings of exceptional points out of Dirac cones," Nature **525**, 354–358 (2015).
119. Y. Li, S. Kita, P. Muñoz, O. Reshef, D. I. Vulis, M. Yin, M. Lončar, and E. Mazur, "On-chip zero-index metamaterials," Nat. Photonics **9**, 738–742 (2015).
120. B. Yang, Q. Guo, B. Tremain, L. E. Barr, W. Gao, H. Liu, B. Barr, Y. Xiang, D. Fan, A. P. Hibbins, and S. Zhang, "Direct observation of topological surface-state arcs in photonic metamaterials," Nat. Commun. **8**, 97 (2017).
121. J. Noh, S. Huang, D. Leykam, Y. Chong, K. P. Chen, and M. Rechtsman, "Experimental observation of optical Weyl points and Fermi arc-like surface states," Nat. Phys. **13**, 611–617 (2017).
122. F. Li, X. Huang, J. Lu, J. Ma, and Z. Liu, "Weyl points and Fermi arcs in a chiral phononic crystal," Nat. Phys. **14**, 30–34 (2018).
123. Y. Lu, N. Jia, L. Su, C. Owens, G. Juzeliūnas, D. I. Schuster, and J. Simon, "Probing the Berry curvature and Fermi arcs of a Weyl circuit," Phys. Rev. B **99**, 020302 (2019).
124. J. Jin, X. Yin, L. Ni, M. Soljačić, B. Zhen, and C. Peng, "Topologically enabled ultrahigh-*Q* guided resonances robust to out-of-plane scattering," Nature **574**, 501–504 (2019).
125. C. W. Hsu, B. Zhen, J. Lee, S.-L. Chua, S. G. Johnson, J. D. Joannopoulos, and M. Soljačić, "Observation of trapped light within the radiation continuum," Nature **499**, 188–191 (2013).
126. K. Hirose, Y. Liang, Y. Kurosaka, A. Watanabe, T. Sugiyama, and S. Noda, "Watt-class high-power, high-beam-quality photonic-crystal lasers," Nat. Photonics **8**, 406–411 (2014).
127. Z. Liu, Y. Xu, Y. Lin, J. Xiang, T. Feng, Q. Cao, J. Li, S. Lan, and J. Liu, "High-*Q* quasibound states in the continuum for nonlinear metasurfaces," Phys. Rev. Lett. **123**, 253901 (2019).
128. X. Yin, J. Jin, M. Soljačić, C. Peng, and B. Zhen, "Observation of topologically enabled unidirectional guided resonances," Nature **580**, 467–471 (2020).
129. D. Taillaert, P. Bienstman, and R. Baets, "Compact efficient broadband grating coupler for silicon-on-insulator waveguides," Opt. Lett. **29**, 2749–2751 (2004).
130. H. Zhou, B. Zhen, C. W. Hsu, O. D. Miller, S. G. Johnson, J. D. Joannopoulos, and M. Soljačić, "Perfect single-sided radiation and absorption without mirrors," Optica **3**, 1079–1086 (2016).
131. L. Allen, M. W. Beijersbergen, R. J. C. Spreeuw, and J. P. Woerdman, "Orbital angular momentum of light and the transformation of Laguerre–Gaussian laser modes," Phys. Rev. A **45**, 8185–8189 (1992).
132. S. Iwahashi, Y. Kurosaka, K. Sakai, K. Kitamura, N. Takayama, and S. Noda, "Higher-order vector beams produced by photonic-crystal lasers," Opt. Express **19**, 11963–11968 (2011).
133. C. Huang, C. Zhang, S. Xiao, Y. Wang, Y. Fan, Y. Liu, N. Zhang, G. Qu, H. Ji, J. Han, L. Ge, Y. Kivshar, and Q. Song, "Ultrafast control of vortex microlasers," Science **367**, 1018–1021 (2020).
134. B. Wang, W. Liu, M. Zhao, J. Wang, Y. Zhang, A. Chen, F. Guan, X. Liu, L. Shi, and J. Zi, "Generating optical vortex beams by momentum-space polarization vortices centred at bound states in the continuum," Nat. Photonics **14**, 623–628 (2020).
135. Z.-Q. Yang, Z.-K. Shao, H.-Z. Chen, X.-R. Mao, and R.-M. Ma, "Spin-momentum-locked edge mode for topological vortex lasing," Phys. Rev. Lett. **125**, 013903 (2020).
136. L.-H. Wu and X. Hu, "Scheme for achieving a topological photonic crystal by using dielectric material," Phys. Rev. Lett. **114**, 223901 (2015).
137. Z. Zhang, X. Qiao, B. Midya, K. Liu, J. Sun, T. Wu, W. Liu, R. Agarwal, J. M. Jornet, S. Longhi, N. M. Litchinitser, and L. Feng, "Tunable topological charge vortex microlaser," Science **368**, 760–763 (2020).